Article

Structure

The LisH Motif of Muskelin Is Crucial for Oligomerization and Governs Intracellular Localization

Graphical Abstract

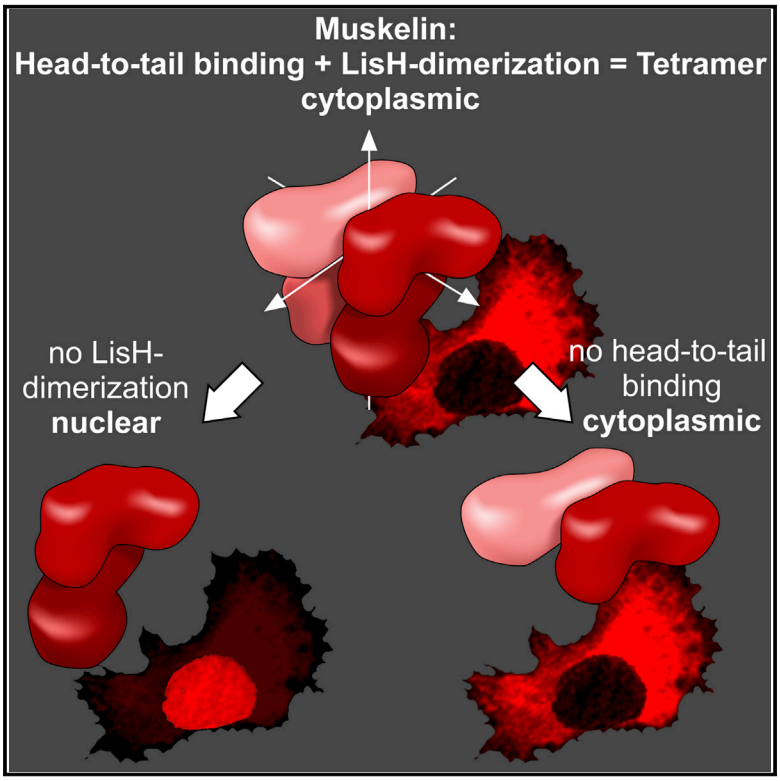

Authors

Carolyn F. Delto, Frank F. Heisler, ..., Matthias Kneussel, Hermann Schindelin

Correspondence

hermann.schindelin@virchow.uni-wuerzburg.de

In Brief

Muskelin organizes the retrograde transport of certain $GABA_A$ receptors. In the crystal structure of the N-terminal discoidin domain and LisH motif, Delto et al. observe a LisH-mediated dimer. They demonstrate that this interaction is required for muskelin tetramerization and determines cellular localization of muskelin.

Highlights

- The LisH motif of muskelin acts as a dimerization interface
- The generic binding site in the discoidin domain mediates a head-to-tail interaction
- Muskelin forms a tetramer as a dimer of dimers via both interfaces
- An impaired LisH dimerization relocates muskelin from the cytoplasm to the nucleus

Accession Numbers

4OYU

Delto et al., 2015, Structure *23*, 364–373
February 3, 2015
http://dx.doi.org/10.1016/j.str.2014.11.016

CellPress

CellPress

Structure
Article

The LisH Motif of Muskelin Is Crucial for Oligomerization and Governs Intracellular Localization

Carolyn F. Delto,[1] Frank F. Heisler,[2] Jochen Kuper,[1] Bodo Sander,[1] Matthias Kneussel,[2] and Hermann Schindelin[1,*]
[1]Rudolf Virchow Center for Experimental Biomedicine, University of Würzburg, D-97080 Würzburg, Germany
[2]Center for Molecular Neurobiology, ZMNH, University Medical Center Hamburg-Eppendorf, D-20251 Hamburg, Germany
*Correspondence: hermann.schindelin@virchow.uni-wuerzburg.de
http://dx.doi.org/10.1016/j.str.2014.11.016

SUMMARY

Neurons regulate the number of surface receptors by balancing the transport to and from the plasma membrane to adjust their signaling properties. The protein muskelin was recently identified as a key factor guiding the transport of α1 subunit-containing $GABA_A$ receptors. Here we present the crystal structure of muskelin, comprising its N-terminal discoidin domain and Lis1-homology (LisH) motif. The molecule crystallized as a dimer with the LisH motif exclusively mediating oligomerization. Our subsequent biochemical analyses confirmed that the LisH motif acts as a dimerization element in muskelin. Together with an intermolecular head-to-tail interaction, the LisH-dependent dimerization is required to assemble a muskelin tetramer. Intriguingly, our cellular studies revealed that the loss of this dimerization results in a complete redistribution of muskelin from the cytoplasm to the nucleus and impairs muskelin's function in $GABA_A$ receptor transport. These studies demonstrate that the LisH-dependent dimerization is a crucial factor for muskelin function.

INTRODUCTION

γ-Aminobutyric acid (GABA) is the major inhibitory neurotransmitter in the mammalian CNS, and the regulation of GABAergic transmission is a fundamental mechanism adapting neuronal excitability. The efficacy of GABAergic transmission critically depends on the number of postsynaptic $GABA_A$ receptors, which is in turn determined by the balance of the transport processes for delivery, removal, and recycling of these receptors (Vithlani et al., 2011). Thus, the identification of factors that regulate the intracellular transport of receptors and thereby maintain this balance is crucial for our understanding of neuronal function. In a recent study, the protein muskelin has been identified as a key regulator of the transport of α1 subunit-containing $GABA_A$ receptors (Heisler et al., 2011), guiding these receptors through the steps required for their removal and degradation. Hence, an altered synchronization of neuronal network activity was observed in hippocampal slices of muskelin knockout mice.

Muskelin is a multidomain protein with a unique domain composition, consisting of an N-terminal discoidin domain followed by a Lis1-homology (LisH) motif, a C-terminal to LisH (CTLH) domain, a kelch domain with six repeats of the kelch motif, and a nonannotated C-terminal module (Figure 1). The protein has been initially identified by its role in the cellular response to the extracellular matrix component thrombospondin-1 (Adams et al., 1998). Several additional binding partners of muskelin have since been reported (Debenedittis et al., 2011; Hasegawa et al., 2000; Ledee, 2005), among them RanBPM and Twa1, with which it forms part of the CTLH complex (Kobayashi et al., 2007; Umeda et al., 2003). The variety of interaction partners matches the widespread expression of muskelin in most tissues (Prag et al., 2007; Tagnaouti et al., 2007).

One common thread between the different functional contexts of muskelin is the involvement in the regulation of transport processes and cytoskeletal organization. Importantly, the role in $GABA_A$ receptor transport suggests that muskelin belongs to a novel class of regulators coordinating transport processes across different cytoskeletal systems. This is also supported by the observation that muskelin knockout mice undergo a change in fur color (Heisler et al., 2011). Fur color depends on the distribution of melanosomes within skin cells (Barral and Seabra, 2004), and trafficking of melanosomes requires an elaborate interplay of both actin- and microtubule-dependent transport (Rodionov et al., 2003; Watabe et al., 2008). The exact function of muskelin, however, remains unclear and the details of how it is regulated are elusive.

One prominent feature of muskelin is its ability to form oligomers. It has been shown that muskelin assembles into a large oligomer in vitro (Kiedzierska et al., 2008) and that the N-terminal discoidin domain can bind to a C-terminal region in a head-to-tail interaction (Prag et al., 2004). Moreover, muskelin also contains a LisH motif, which so far has not been considered in the context of muskelin oligomerization. A LisH-dependent dimerization has been observed for several proteins (Kim et al., 2004; Mikolajka et al., 2006; Oberoi et al., 2011) and has thus been suggested to be a general feature of proteins containing this motif. Interestingly, a study of several disease-causing mutations revealed that the LisH dimerization can be of vital importance for protein function, as a loss of the ability to dimerize has a severe impact on protein half-life and localization (Gerlitz et al., 2005). However, neither the role of the LisH motif in muskelin oligomerization nor its functional impact has been investigated.

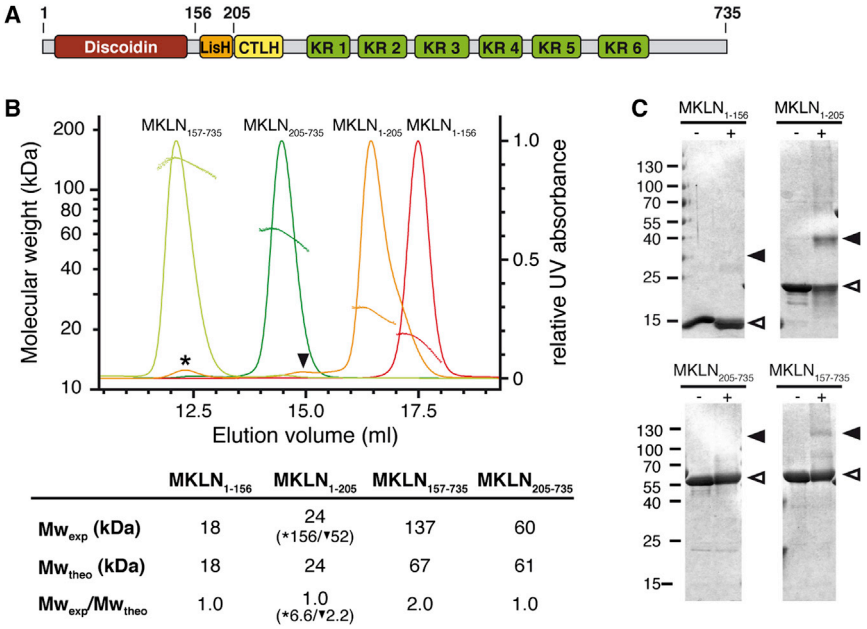

	$MKLN_{1-156}$	$MKLN_{1-205}$	$MKLN_{157-735}$	$MKLN_{205-735}$
Mw_{exp} (kDa)	18	24 (*156/▾52)	137	60
Mw_{theo} (kDa)	18	24	67	61
Mw_{exp}/Mw_{theo}	1.0	1.0 (*6.6/▾2.2)	2.0	1.0

Figure 1. The LisH Motif Mediates Dimerization

(A) Domain architecture of muskelin with borders of truncated constructs indicated.

(B) SEC-MALS analyses identify $MKLN_{157–735}$ and a small portion of $MKLN_{1–205}$ as dimers. Molar masses are overlaid with the A_{280} elution profiles in the upper graph. Experimental (Mw_{exp}) and theoretical molecular weights (Mw_{theo}) and their ratio are summarized in the table. For $MKLN_{1–205}$, two small peaks precede the main peak (asterisk and arrowhead) and were considered during analysis.

(C) BS^3 crosslinks $MKLN_{1–205}$ and $MKLN_{157–735}$, but not $MKLN_{1–156}$ and $MKLN_{205–735}$, to their dimeric forms. The SDS-PAGE of the fractionated crosslinking reactions and controls are shown, with arrowheads indicating the expected position of the respective monomer (open) and dimer (filled).

Here we present the crystal structure of muskelin's N-terminal part, the discoidin domain and LisH motif. This crystal structure provided the molecular details for a comprehensive biochemical analysis of muskelin oligomerization and allowed the investigation of the impact of oligomerization on muskelin's function in different cellular contexts.

RESULTS

LisH Is a Dimerization Motif in Muskelin

To analyze the role of the individual domains in muskelin oligomerization, we prepared a set of truncated muskelin variants sequentially shortened by one domain from either the N- or the C-terminus. Based on secondary structure predictions obtained with Phyre (Kelley and Sternberg, 2009), we positioned the boundaries in putatively unstructured regions (Figure 1A). We first addressed the question of whether the LisH motif acts as a dimerization motif in muskelin. Therefore, we compared the ability to dimerize of the truncated constructs including the LisH motif ($MKLN_{1–205}$ and $MKLN_{157–735}$) with those without it ($MKLN_{1–156}$ and $MKLN_{205–735}$) by size-exclusion chromatography coupled with multiangle laser light scattering (SEC-MALS) and chemical crosslinking.

The molecular masses derived by MALS analysis for the constructs without the LisH motif ($MKLN_{1–156}$ and $MKLN_{205–735}$) are in very good agreement with the theoretical molecular mass of the respective monomers (Figure 1B). For N-terminally truncated $MKLN_{157–735}$, which still includes the LisH motif, the derived molecular mass matches that of a dimer. In contrast, for $MKLN_{1–205}$ the dominant species is monomeric and only a very small dimer fraction (highlighted by an arrowhead in Figure 1B) was detected at mean concentrations of 5 μM and 0.15 μM in the monomer and dimer peaks, respectively. This indicates a weak dimerization of $MKLN_{1–205}$ for which the monomer-dimer equilibrium is shifted to the monomeric form at the concentration analyzed.

The dimerization capabilities of the domain constructs were further probed by crosslinking with the amine-sensitive bis[sulfosuccinimidyl]suberate (BS^3) reagent; a band for the crosslinked dimeric form could be observed only for $MKLN_{157–735}$ and $MKLN_{1–205}$ (Figure 1C). Again, for the truncated constructs without the LisH motif ($MKLN_{1–156}$ and $MKLN_{205–735}$) only the monomer was detected. Notably, $MKLN_{1–205}$, which was found as predominantly monomeric by SEC-MALS, is crosslinked very efficiently into its dimeric form. Thus, both methods unequivocally show that constructs containing the LisH motif are able to form dimers, confirming that the LisH motif is a functional dimerization element in muskelin.

Crystal Structure of $MKLN_{12–205}$

We were able to grow crystals of the $MKLN_{1–205}$ fragment, which is composed of the discoidin domain and the LisH motif. Although the crystals diffracted to high resolution (1.7 Å) and phasing was possible through sulfur-based single-wavelength anomalous diffraction (SAD) experiments, refinement of the model did not yield a free R factor below 34%, thus indicating an inherent problem. To improve the crystals we truncated the N-terminus, removing residues that were disordered in the initial structure. The shortened $MKLN_{12–205}$ construct crystallized in space group $P2_12_12_1$, and the crystals diffracted up to 1.8 Å resolution. The structure was solved by molecular replacement with the model derived for $MKLN_{1–205}$. The final model contained residues 12–187 and refinement resulted in an R factor of 15.6% (R_{free} = 19.3%) with good stereochemistry (Table 1). Comparison of the preliminary model of $MKLN_{1–205}$ with the final refined model for $MKLN_{12–205}$ revealed that the two structures are very similar, with a root mean square deviation of 0.39 Å, despite the poor refinement statistics of $MKLN_{1–205}$.

The overall structure shows that $MKLN_{12–205}$ forms a dimer, with the dimer interface located solely in the LisH motif (Figure 2A). The discoidin domain adopts the typical jellyroll fold, in which a five-stranded antiparallel β sheet is

Table 1. Data Collection, Phasing, and Refinement Statistics

	$MKLN_{12–205}$	$MKLN_{1–205}$	
		Native	Sulfur SAD
Data Collection Statistics			
Wavelength (Å)	0.95373	0.91841	1.9
Resolution range (Å)	33.8–1.8 (1.9–1.8)	65.1-1.7 (1.79–1.7)	34.1–2.28 (2.4–2.28)
Space group	$P2_12_12_1$	$P4_32_12$	$P4_32_12$
Unit cell (Å)	a = 63.06, b = 65.3, c = 101.39	$a = b$ = 65.15, c = 101.53	$a = b$ = 64.99, c = 101.56
Total reflections	176855	106685	447829
Unique reflections	39509 (5686)	24751 (3535)	10549 (1498)
Multiplicity	4.5 (4.5)	4.3 (3.9)	42.5 (36.7)
Completeness (%)	100.00 (100.00)	100.00 (100.00)	100.00 (100.00)
Mean I/σ (I)	17.0 (4.7)	9.6 (1.8)	30.0 (6.5)
Wilson B factor (Å^2)	26.4	25.0	43.9
R_{merge}[a]	4.9 (30.1)	6.9 (67.6)	9.6 (90.9)
Phasing Statistics			
Figure of merit			0.324
Number of sites			9
Refinement Statistics			
R factor	0.1562 (0.1974)		
R_{free}	0.1931 (0.2313)		
Number of atoms	3398		
Macromolecules	3019		
Ligands	102		
Water	277		
Protein residues	357		
RMS deviations in			
Bond lengths (Å)	0.014		
Bond angles (°)	1.42		
Ramachandran favored (%)	96		
Ramachandran outliers (%)	0		
Clashscore	13.94		
Average B factor (Å^2)	41.2		
Macromolecules	40.2		
Solvent	47.1		

Statistics for the highest-resolution shell are shown in parentheses. Ramachandran statistics have been determined with MolProbity (Davis et al., 2004) and refer to the percentage of residues in the core/allowed/disallowed regions of the Ramachandran diagram.

[a] $R_{merge} = \sum_{hkl}\sum_k|I(k) - [I]|/\sum_{hkl}\sum_k I(k)$, where $I(k)$ is the value of the k^{th} measurement of the intensity of a reflection, $[I]$ is the mean value of the intensity of that reflection, and the summation is over all measurements. $R = \sum_{hkl}|F_{obs} - F_{calc}|/\sum_{hkl}|F_{obs}|$, where F_{obs} and F_{calc} are the observed and calculated structure factors, respectively, for all data (no σ cutoff). $R_{free} = R$ calculated with 5% of the reflection data chosen randomly and omitted prior to the start of refinement.

sandwiched against a three-stranded antiparallel β sheet and the strands are connected by long, flexible loops. The arrangement agrees well with known structures of the discoidin domain family (Figure S1 available online). It should be noted that none of the four cysteines located in the discoidin domain is within suitable distance to form a disulfide bridge as proposed earlier (Kiedzierska et al., 2007, 2008). An extended α helix follows at the C-terminus of the discoidin domain, which directly leads into the predicted first helix of the LisH motif. At the end of this helix, only two more residues were visible while the remaining half of the LisH motif could not be resolved.

The Dimerization Interface in the Crystal Structure

The extended α helices of the protomers run antiparallel and are slightly twisted. The residues of the C-terminal part, which correspond to the first helix of the canonical LisH motif, interdigitate and form a tight interface (Figure 2B). Among the corresponding side chains, Cys180 from both monomers lie closest to each other and mark the center of the interface. Several hydrophobic residues contribute to the interface, most prominently Phe184, and additionally Ala176, Ile177, and Leu181. Furthermore, hydrogen bonds and salt bridges created by Glu173 and Arg185 stabilize the dimer (Table S1, based on a PISA analysis; Krissinel and Henrick, 2007).

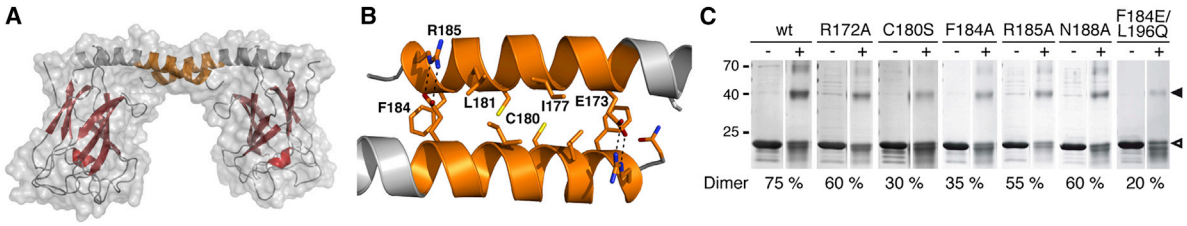

Figure 2. Molecular Details of the LisH-Mediated Dimerization

(A) Crystal structure of the $MKLN_{12–205}$ dimer in ribbon representation superimposed with a semitransparent molecular surface. Secondary structure elements are colored red for the discoidin domain and orange for the LisH motif. See also Figure S1.

(B) Close-up view of the dimer interface, with residues mediating dimerization in stick representation and hydrogen bonds shown as dashed lines. See also Figure S2 and Table S1.

(C) SDS-PAGE of the crosslinking reactions. For each $MKLN_{1–205}$ variant (indicated on top), the control sample without (−) and the sample with (+) crosslinker is shown, and the fraction of crosslinked dimer is given below. Arrowheads indicate the expected position of the respective monomer (open) and dimer (filled). Multiple bands for the monomer appearing upon crosslinking are presumably caused by intramolecular crosslinks.

Comparing the partial LisH motif of muskelin with the homologous structures of Lis1, FOP, and TBL1 (Kim et al., 2004; Mikolajka et al., 2006; Oberoi et al., 2011) reveals noteworthy differences. Although the underlying interaction principle, namely two antiparallel helices forming a mainly hydrophobic interface, is the same, the arrangement of the helices differs fundamentally; the rotation of the helices with respect to each other is in the opposite direction. In a side view of the two helices, the backward helix is rotated counterclockwise by ~130°–140° for Lis1, FOP, and TBL1, but clockwise by ~140° in muskelin (Figure S2A), with axes of rotation at homologous positions (centered between the following residues: Cys180 in muskelin, Ile15 in Lis1, Val12 in TBL1, and Val78 in FOP). Moreover, the second half of the LisH motif could not be resolved in our structure. In the canonical LisH motif, the second helix folds back onto the first helix and dimerization results in a four-helix bundle. As symmetry mates occupy the space on top of the first helix, where the second helix would be expected in a canonical arrangement, we cannot rule out that this arrangement is prevented by crystal contacts. However, the fact that the second helix was not visible could indicate that these residues are flexible and, hence, this would be another deviation from the generic LisH architecture. Interestingly, the presence of the second helix was a prerequisite for dimerization and crystallization, as a construct lacking the second helix, $MKLN_{1–187}$, was both impaired in dimerization (Figure S2B) and did not crystallize. It should be noted that one of the most highly conserved residues among LisH motifs, a glutamate at the C-terminal end of the second helix, is replaced by a lysine (Lys198) in muskelin (Figure S2C, position 28). This glutamate fulfills a vital role in all known structures, stabilizing the antiparallel arrangement of the second helix in the dimer by hydrogen bonds with the backbone amides of the N-terminal residues in the opposing helix and a favorable charged interaction with the helix dipole (Figure S2D). The lysine at the homologous position in muskelin can fulfill neither of these specific roles, thus supporting the notion that the LisH motif in muskelin may deviate in its stability and architecture from other LisH motifs.

Mutations in the LisH Motif Impede Dimerization

To probe the dimerization interface revealed by our structure, we introduced several mutations into the first helix of the LisH motif. Moreover, we aimed to design a dimerization-deficient variant and therefore targeted a major contributor, Phe184, and exchanged it with a glutamate to disrupt the hydrophobic core. To further weaken the dimer, by breaking up a secondary point in the interface and impede the contribution of the second helix, we additionally replaced the conserved Leu196 with a glutamine.

We analyzed the dimerization of the $MKLN_{1–205}$ variants by chemical crosslinking (Figure 2C). Based on the fraction of dimer that is crosslinked, dimerization impairment of the individual mutations can be put in the following, ascending order: N188A ≈ R172 < R185A < F184A < C180S < F184E/L196Q. Thus, the effect of each mutation was in good agreement with the contribution of the respective residue to the interface as estimated by the buried surface area and the gain in free energy upon dimerization (Table S1). As intended, the F184E/L196Q double mutant showed

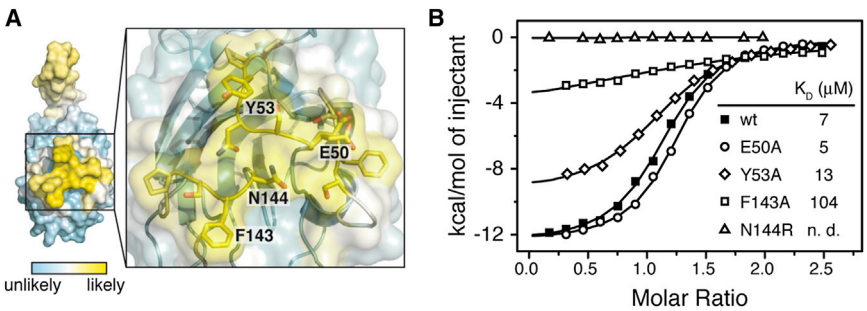

Figure 3. The Main Determinants of the Head-to-Tail Binding Are Located in the β7-β8 Loop

(A) The Meta-PPISP score indicative of a protein-protein interaction interface is displayed as a color value on the surface of the $MKLN_{12–205}$ monomer with a close-up view into the identified interaction site. Residues with a score above 0.45 are shown in stick representation.

(B) Binding isotherms obtained by ITC in which $MKLN_{205–735}$ was titrated with different $MKLN_{1–156}$ variants. Binding enthalpies are plotted as a function of the molar ratio of the binding partners and dissociation constants are summarized. See also Figure S3.

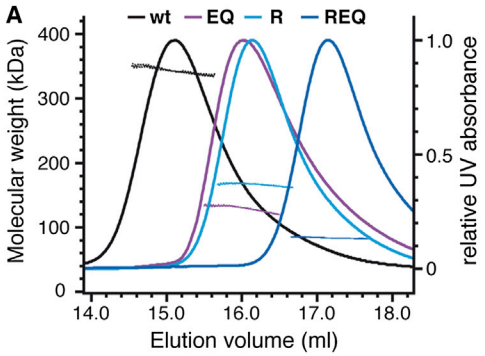

	wt	EQ	R	REQ
Mw_{exp}(kDa)	344	130	167	84
Mw_{exp}/Mw_{mono}	4.1	1.5	2.0	1.0
Mw_{theo}(kDa)	339	170	170	85

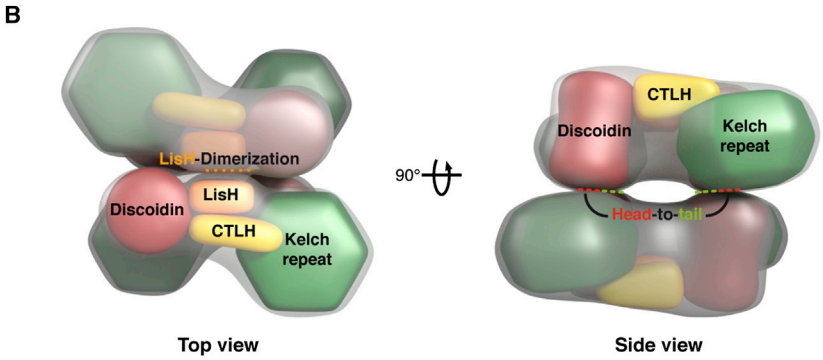

Figure 4. SEC-MALS Analyses Show the Stepwise Breakup of the Muskelin Oligomer

(A) Molar masses obtained as a function of elution volume are overlaid with the respective A_{280} elution profile (left). Experimental molecular weights (Mw_{exp}), the ratio of experimental and theoretical molecular weight of the monomer (Mw_{mono}), and the theoretical molecular weights (Mw_{theo}) of the respective oligomer are given on the right.

(B) Model of the muskelin tetramer. Monomers are depicted with gray semitransparent surfaces, with the domains being color coded as in Figure 1 and the interaction interfaces indicated by dashed lines. See also Figure S4.

a substantially weakened dimerization and was therefore used in later analyses to investigate the role of the LisH dimerization.

The Head-to-Tail Interaction Can Be Abolished by a Single Point Mutation

After having confirmed that the LisH motif acts as a functional dimerization element, we also wanted to dissect the previously reported head-to-tail interaction of the discoidin domain with the C-terminal part of muskelin (Prag et al., 2004). Based on our structure of the N-terminal part of muskelin, we used the meta-PPISP server (Qin and Zhou, 2007) to identify potential binding sites located in the discoidin-like domain. As expected, residues Ser169 to Asn188 were identified as a potential protein-protein interface, perfectly matching the dimerization interface in the LisH motif. Only one additional area was proposed as an interaction site. This site is located at the bottom of the β barrel of the discoidin domain (Figure 3A) and is formed by residues Trp23 to Tyr30 and Glu50 to Pro55 in the loop connecting β strands 1 and 2 and Trp139 to Asn144 in the loop that connects β strands 7 and 8.

We introduced several mutations to test this putative interface and analyzed their effect on the head-to-tail interaction by measuring the binding of the discoidin domain $MKLN_{1–156}$ to the C-terminal construct $MKLN_{205–735}$ in isothermal titration calorimetry (ITC) experiments (Figure 3B). For the wild-type, a dissociation constant of 6.8 μM was determined; the effect of the different mutations ranged from no effect for E50A (K_D = 5 μM), over a weakened binding for Y53A (K_D = 13 μM) and F143A (K_D = 104 μM), up to a reduction of binding to a level that was not detectable by ITC for the N144R mutation. At the same time, we dissected the contributions of the kelch domain and the C-terminal module to the head-to-tail interaction (Figure S3) and found that the C-terminal residues do not play a role in the head-to-tail interaction, which must therefore be mediated solely by the kelch domain interacting with the discoidin domain.

Both Interaction Interfaces Are Needed to Assemble the Oligomer

With the F184E/L196Q and N144R mutations as tools to separately impair the two self-interactions of muskelin, we next dissected their contributions to muskelin oligomerization. We introduced the respective mutations both individually and in combination into the full-length protein and analyzed the oligomeric state of the proteins by SEC-MALS (Figures 4 and S4). Wild-type muskelin eluted earliest and the determined molecular mass was in very good agreement with the mass of a tetramer. The single variants of the respective interfaces eluted in close succession and the molecular mass for the N144R mutation was very close to the mass of the dimer; for the F184E/L196Q variant, the value obtained was intermediate between a dimeric and monomeric form. Finally, the variant with the combination of both interface mutations (triple mutation N144R/F184E/L196Q) eluted last and the determined molecular mass was in good agreement with the theoretical mass of the monomer (84.8 kDa).

The difference between the theoretical mass of a dimer and the experimental value for the F184E/L196Q variant can be accounted for neither by protein degradation nor by unfolding, as protein integrity was confirmed by SDS-PAGE, mass spectrometry, and CD spectroscopy (Figure S5). A possible explanation lies in the fast binding kinetics of the head-to-tail interaction, resulting in a dynamic monomer-dimer mixture that cannot be separated by size-exclusion chromatography and thus interferes with the correct determination of the molecular mass. Nonetheless, the results clearly show that both interactions are required to assemble the tetrameric form of muskelin as a dimer of dimers. In conjunction with our structural data and mapping experiments, this allowed us to construct a possible architecture of the muskelin tetramer (Figures 4 and S4).

The Role of Muskelin's Self-Interactions in a Cellular Context

With the knowledge that the muskelin tetramer is assembled via two dimerization events, we next wanted to dissect the

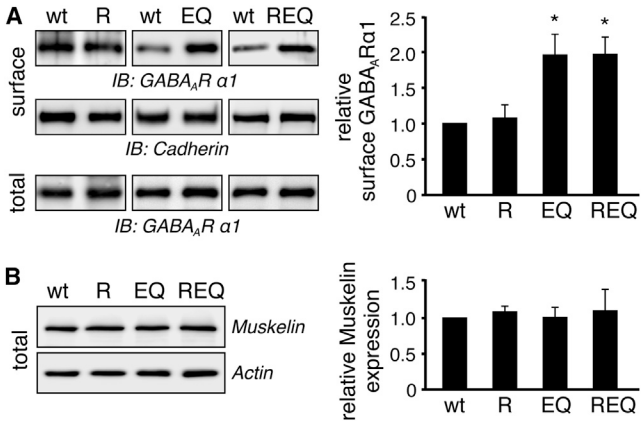

Figure 5. Altered Function of Muskelin Variants

(A) Analysis of GABA$_A$R α1 surface levels upon biotinylation of GABA$_A$R α1 and GABA$_A$ R β3 expressing HEK293 cells. Controls: surface pan cadherin and total GABA$_A$R α1 levels. GABA$_A$R α1 surface levels were analyzed upon co-expression of the N144R variant (R, 1.07 ± 0.17, n = 3), the F184E/L196Q variant (EQ, 1.95 ± 0.28, n = 5), and the N144R/F184E/L196Q variant (REQ, 1.97 ± 0.23, n = 4) always compared with wild-type (set to 1). Student's t test (*$p < 0.05$) was used for statistical analysis.

(B) Total expression levels of wild-type and variant muskelin mCherry-fusion proteins in HEK293 cells. N: 1.05 ± 0.05; EQ: 1.02 ± 0.08; REQ: 1.06 ± 0.13; wild-type set to 1 (n = 5). Control: actin detection. See also Figure S5.

Data are represented as mean values ± SEM.

importance of each interface with respect to the physiological function of muskelin. As muskelin is required for the removal of GABA$_A$ receptors (GABA$_A$R) from the plasma membrane during endocytosis (Heisler et al., 2011), we monitored cell surface levels of GABA$_A$R α1 in the presence of wild-type or mutated muskelin variants. In HEK293 cells, we observed a strong increase in GABA$_A$R α1 surface levels by about 95% upon coexpression of either the F184E/L196Q variant or the N144R/F184E/L196Q variant compared with the wild-type and the N144R variant (Figure 5A). These differences were not caused by altered expression levels of the wild-type and the variants (Figure 5B). To ensure that the detrimental effect of the F184E/L196Q variant, i.e., a loss of LisH dimerization impairs GABA$_A$R α1 transport, was not biased by either folding defects or an impaired binding of muskelin to the receptor subunit, we analyzed folding by CD spectroscopy and binding properties by ITC measurements for the F184E/L196Q variant (Figure S5), and found both properties to be unaltered.

The dependency of GABA$_A$R α1 surface levels on an intact LisH-dependent dimerization prompted us to study the intracellular distribution of the different muskelin variants. Upon expression in HEK293 cells, we observed that the majority of RFP-tagged wild-type muskelin appeared cytoplasmic (Figure 6A), which is in agreement with previous data on muskelin GFP-fusion proteins (Valiyaveettil et al., 2008). A similar distribution of RFP-muskelin was observed when the N144R mutation was introduced. Interestingly, the F184E/L196Q and N144R/F184E/L196Q variants showed a striking redistribution from the cytoplasm to the nucleus after which either fusion protein was hardly detectable at the cell periphery. Quantification revealed that this redistribution applied to the vast majority of cells; an accumulation of muskelin in the nucleus was observed in ~12%–15% of the cells for wild-type and N144R RFP-muskelin, but in ~86%–92% of the cells for the F184E/L196Q and the N144R/F184E/L196Q variant (Figure 6B). This indicates that the intracellular distribution of muskelin is highly regulated by its oligomeric state and is dependent on the LisH-mediated dimerization. The two different dimeric forms of muskelin, assembled from either the head-to-tail or the LisH motif-mediated interaction, exhibit different cellular properties.

We finally asked whether the LisH dimerization would similarly affect muskelin distribution in neurons. Primary hippocampal neurons transfected with mCherry-fusion proteins at days in vitro (DIV) 11–13 were analyzed for their intracellular distribution. Whereas wild-type and N144R mCherry-muskelin appeared to always be enriched in the cytoplasm, the F184E/L196Q and N144R/F184E/L196Q variants showed a clear redistribution into the nucleus (Figure 6C), confirming our results from HEK293 cells.

A change in subcellular localization for mutated or truncated variants of muskelin was reported previously (Valiyaveettil et al., 2008). We therefore included the described K182A/H183A double mutation in the LisH motif and the deletion of the last 35 amino acids at the C-terminus (ΔC35) in our analysis. In neurons, the K182A/H183A mutation had no effect on the cytoplasmic localization of mCherry-muskelin, whereas mCherry-muskelin-ΔC35 showed a mixed nuclear and cytoplasmic distribution. In parallel, we biochemically analyzed these variants to assess their effects on muskelin oligomerization. Unfortunately both variants, the K182A/H183A and the ΔC35 deletion, were prone to aggregation and degradation. The ΔC35 deletion was inseparable from chaperones and could not be purified in sufficient quantity and quality. We therefore investigated the effect of the C-terminus with a construct ending after amino acid 625, corresponding to a deletion of the complete 110 amino acid long C-terminal module (ΔC110). Notably, an analysis of full-length muskelin harboring either the K182A/H183A mutation or ΔC110 deletion by SEC-MALS revealed that both variants prevented muskelin tetramerization. The detected masses corresponded to a dimer/monomer mixture, with the predominant species being the dimer in the case of the K182A/H183A mutation and the monomer in the case of the ΔC110 deletion (Figure S6). This revealed that the C-terminus is a further factor influencing muskelin oligomerization, which thus seems to depend on an intricate interplay of several domains in muskelin. Moreover, this opens the possibility that the observed effect of the C-terminus on the cellular localization of muskelin is caused by or mediated via its role in oligomerization.

DISCUSSION

Until now it was only known that muskelin is able to oligomerize and undergo a head-to-tail interaction, which likely contributes to oligomerization (Kiedzierska et al., 2008; Prag et al., 2004). However, the presence of a LisH motif in muskelin prompted us to speculate that oligomerization could be a multifactorial process and may have a direct impact on its function. We therefore analyzed the role of the LisH motif and revealed by structural and biochemical analyses that it acts as a dimerization element in muskelin and is required for oligomerization. Furthermore, we

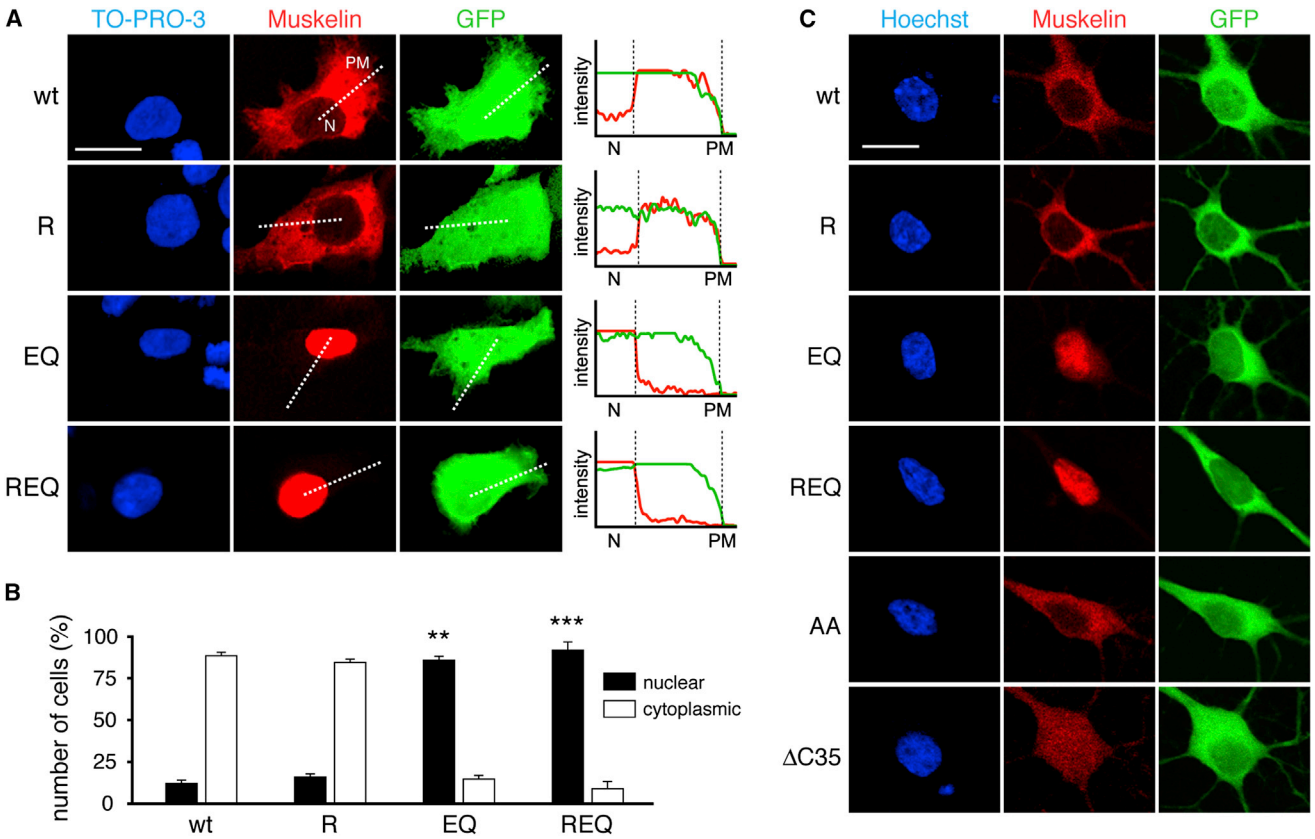

Figure 6. Altered Intracellular Distribution of Muskelin Variants

(A) Confocal imaging (GFP coexpression was used to identify cell boundaries; nuclei were labeled using TO-PRO-3). Scale bar, 15 μm; dashed lines indicate traces used for line scans shown on the right. N, nucleus; PM, plasma membrane.

(B) Localization analysis of wild-type and variant muskelin RFP-fusion proteins in HEK293 cells (wild-type, 11.7% ± 1.2% nuclear and 88.3% ± 1.2% cytoplasmic; R, 15.7% ± 1.0% nuclear and 84.3% ± 1.0% cytoplasmic; EQ, 85.6% ± 1.6% nuclear and 14.4% ± 1.6% cytoplasmic; REQ, 92.3% ± 2.7% nuclear and 7.7% ± 2.7% cytoplasmic, n = 3). Student's t test (***$p < 0.001$; **$p < 0.01$) was used for statistical analysis. Data are represented as mean values ± SEM.

(C) Analysis of wild-type and variant muskelin mCherry-fusion proteins in DIV 11–13 hippocampal neurons (GFP coexpression was used to identify cell boundaries, nuclei were labeled using Hoechst 33342). Scale bar, 15 μm. Neurons from four independent experiments were analyzed. See also Figure S6.

showed that the LisH-mediated dimerization determines the subcellular localization of the protein and is essential for muskelin function.

Our data clearly reveal that the LisH motif (Emes and Ponting, 2001) mediates critical interactions for a homodimerization of muskelin, as point mutations within this motif abolish dimer formation. However, the substantially weaker dimerization of $MKLN_{1–205}$ compared with $MKLN_{157–735}$ and the full-length protein (Figures 1B and 4) indicates that the LisH-dependent dimerization is further stabilized by elements residing in the C-terminal part of muskelin. This is in line with observations on other LisH motif-containing proteins in which the LisH motif is the primary dimerization interface, yet the dimerization is further supported by other parts of the respective proteins (Kim et al., 2004; Mateja et al., 2006; Mikolajka et al., 2006; Oberoi et al., 2011).

Surprisingly, in our crystal structure the arrangement of the LisH motif deviates substantially from known structures of LisH family members (Kim et al., 2004; Mikolajka et al., 2006; Oberoi et al., 2011). Key features are retained; the N-terminal part forms an α helix, which dimerizes with its symmetry equivalent, and within the interface the intersection point and the participating residues are at homologous positions. However, the topology differs substantially in that the rotation between the two helices in the dimer is inverted compared with other LisH family members. In addition, the ensuing residues, which form a second α helix in the LisH family, were not visible in our crystal structure; nevertheless, our results obtained with a shortened construct lacking the second helix confirmed that it contributes to dimerization. A notable difference of muskelin from known LisH structures is the replacement of a highly conserved glutamate at the C-terminus of the second helix by a lysine in muskelin (Figure S2C, position 28 of the motif). The high degree of conservation of this glutamate is matched by its important structural role in the LisH motif (Figure S2D). The absence of this glutamate is indicative of a less stable or differing arrangement of the helices in muskelin. Together with the observation that the homodimerization via the LisH motif is supported by the C-terminal part of muskelin, this corroborates the assumption that the LisH motif in muskelin needs to be embedded in and stabilized by the environment of the protein to fulfill its function in dimerization.

Although dimerization of muskelin via its LisH motif has not been detected, the ability of muskelin's discoidin domain to

bind to muskelin's C-terminal portion had been previously reported (Prag et al., 2004). However, thus far it has not been demonstrated that this interaction represents a direct binding event or that it contributes to the oligomer observed in vitro. Based on our structural data combined with biochemical analyses, we were able to identify residues critical for the interaction in the loops connecting β strands 1 and 2 as well as β strands 7 and 8 of the discoidin domain. Our mapping coincides with the common binding site of discoidin domains, and as discoidin domains typically bind one ligand specifically (Kiedzierska et al., 2007), we conclude that the natural ligand of muskelin's LisH domain is the C-terminus of muskelin. While a contribution of discoidin domains to protein oligomerization via the formation of disulfide bridges (Wu et al., 2005) has been reported before, our study identifies an example of a discoidin domain that mediates an oligomerization via direct binding with its specific binding site.

Muskelin has been shown to form a large oligomer in vitro, assigned by size-exclusion chromatography as hexamer (Kiedzierska et al., 2008). In contrast, we deduced by MALS a significantly smaller mass corresponding precisely to a tetramer. The deviations are likely to be explained by the techniques used; size-exclusion chromatography is influenced by molecular shape, whereas static light scattering directly measures molecular mass (Wen et al., 1996). Furthermore, with the aid of our self-interaction-impairing mutations, we observed the stepwise disassembly of the muskelin tetramer and found that both interactions are independently required to assemble the muskelin tetramer as a dimer of dimers. Combining these observations with the structural information and the mapping of the interfaces, we have conceived a possible model for the arrangement of the muskelin oligomer (Figures 4 and S4) that helps to envision the different oligomeric states of muskelin: tetramer, LisH dimer, head-to-tail dimer, and monomer. Apart from providing insights into the assembly of the oligomer, our analyses verified that the mutations we introduced are suitable tools for analysis of the functional relevance of muskelin oligomerization. Each variant abolished one of the interactions underlying oligomerization while no detrimental effects on the stability or folding of the protein were detected.

With these tools, we demonstrated that LisH-mediated dimerization is of vital importance for muskelin function. We observed a significant increase in $GABA_A$ receptor surface levels, indicating reduced receptor internalization for the LisH-dimerization-impaired variant in cotransfected HEK293 cells. This effect seems to be ultimately due to an altered intracellular distribution of these variants. Muskelin was previously described as a nucleocytoplasmic protein that is found mainly distributed throughout the cytoplasm (Adams et al., 1998; Hasegawa et al., 2000; Heisler et al., 2011; Ledee, 2005) and to a lesser extent in the nucleus (Tagnaouti et al., 2007; Valiyaveettil et al., 2008). Interference with the LisH-mediated dimerization resulted in a striking redistribution of muskelin to the nucleus as shown in HEK293 cells and hippocampal neurons. This finding is in line with results of an earlier study of three LisH-containing proteins, for which an impaired LisH-dependent dimerization in every case led to a change in localization of the protein and a dramatic decrease in protein half-life (Gerlitz et al., 2005).

It is interesting that of the two interactions underlying muskelin oligomerization, we observed effects on muskelin function only for the LisH-mediated dimerization but not for the head-to-tail interaction. A regulatory mechanism for the head-to-tail interaction via phosphorylation by protein kinase C has already been proposed (Prag et al., 2007), which suggests that this interaction is also a target for adaptation of muskelin function. It remains open whether other functional readouts are needed to detect the effect of an impaired head-to-tail interaction. Since it is not trivial to assess the oligomeric state in the cell, we cannot rule out that, in the cellular assays used, the head-to-tail interaction is per se inactivated and thus the effects of a disturbed interaction would be concealed.

The mechanism how the loss in LisH-dependent dimerization leads to a relocalization is currently unknown. Muskelin does not contain any classical nuclear localization signal (NLS) sequence nor is an NLS signal generated by the mutations we introduced. Moreover, a Crm1-dependent export of muskelin from the nucleus, which could be disturbed by the loss of dimerization, has already been excluded in an earlier study (Valiyaveettil et al., 2008). One scenario would be either an impaired or enhanced binding of muskelin to one of its interaction partners resulting from the loss of LisH-dependent dimerization. Candidates include RanBP9 or other components of the CTLH complex, especially in light of the aforementioned study (Valiyaveettil et al., 2008), which observed a nuclear localization activity of the LisH motif depending on a complex interplay with the C-terminus, which also mediates the interaction with RanBP9.

The parallel between LisH dimerization determining the intracellular localization in our hands and the nuclear localization activity noted previously prompted us to investigate the effect of the variants presented in the earlier study (Valiyaveettil et al., 2008). The effect on muskelin localization in a neuronal background differs from the earlier description, since mutation of the basic residues (K182A/H183A) did not change the intracellular distribution and deletion of the last 35 amino acids resulted in a mixed distribution, not a complete nuclear localization as reported before. Notably, our biochemical analyses showed surprising effects of the missing C-terminus and the K182A/H183A mutation on muskelin oligomerization. A stipulatory model is that the very C-terminal part of muskelin facilitates the LisH-dependent dimerization without directly mediating it, in line with the general observation that LisH-dependent dimerization usually requires additional stabilization as discussed above. It would also provide a possible explanation for the effect of the K182A/H183A mutation. While the mutated residues are not part of the dimer interface (Table S1), they could possibly be involved in stabilizing the interaction with the C-terminus. Finally, the effect on the head-to-tail interaction, which is apparently prevented in the absence of the C-terminus, cannot be explained with the data in hand, but one can speculate that the C-terminus may have a profound effect on the arrangement of the domains in the oligomer. While the details of the apparent interplay of the domains in muskelin oligomer formation remain speculative, our results clearly show that any effect influencing the intracellular localization and function of muskelin, whether by mutation or post-translational modification, cannot be considered without taking into account the impact on muskelin oligomerization.

The complex domain architecture of muskelin and the intricate interplay of its domains allow for an interesting way of regulating muskelin function. The link between alterations in oligomeric

state and intracellular redistribution demonstrated by our cellular analyses is tight and prominent. This is remarkable in light of muskelin's participation in the CTLH complex, the mammalian homologue of the GID (glucose-induced degradation deficient) complex in *Saccharomyces cerevisiae* (Francis et al., 2013; Regelmann et al., 2003). The components of this complex show striking similarities in their domain architecture and several of them contain the LisH-CTLH tandem. A localization-specific composition of the complex has been proposed, with a cytoplasmic and a nuclear pool (Kobayashi et al., 2007). The estimated 20S size of the complex contradicts an incorporation of muskelin in its tetrameric form. Thus, the recruitment of muskelin into the complex might depend on an altered oligomeric state. Together with the notion that several of the CTLH subunits contain LisH motifs, this suggests a novel mechanism in regulating the composition and, thereby, the function of the whole complex depending on the oligomeric state of its subunits.

EXPERIMENTAL PROCEDURES

Protein Expression and Purification

All muskelin variants were expressed in *Escherichia coli* as His-tagged small ubiquitin-like modifier (SUMO) fusion proteins and were purified via an initial Ni-affinity chromatography followed by removal of the 6xHis-SUMO-tag, an optional anion exchange chromatography, and a final size-exclusion chromatography. Details on the constructions of the expression plasmid and the experimental conditions during expression and purification are described in the Supplemental Experimental Procedures.

Crystallization and Data Collection

Crystals for $MKLN_{1–205}$ and $MKLN_{12–205}$ were obtained at 20°C by hanging drop vapor diffusion against a reservoir solution containing 100 mM BisTris (pH 5.25–6.0), 200 mM NaCl, and 20%–35% PEG 3350 at a protein concentration of 15–20 mg/ml. For cryoprotection, crystals were first transferred into their respective mother liquor containing 15% ethylene glycol, then into mother liquor containing 30% ethylene glycol, and finally flash frozen in liquid nitrogen.

Diffraction data for $MKLN_{1–205}$ were collected at a wavelength of 1.9 Å for the sulfur single-wavelength anomalous diffraction experiment or 0.92 Å for the native data set, respectively, on the BESSY beamline BL14.1 of the Helmholtz Zentrum Berlin on a Rayonix MX225 detector. The data for $MKLN_{12–205}$ were collected on beamline BM14 at the European Synchrotron Radiation Facility synchrotron in Grenoble with a MAR 225 CCD detector at a wavelength of 0.95 Å. Diffraction data were processed with XDS (X-ray Detector Software; Kabsch, 2010) and iMOSFLM (Leslie and Powell, 2007), respectively, resulting in space group $P4_32_12$ with $a = b = 64.99$ (65.15) Å and $c = 101.56$ (101.53) Å for $MKLN_{1–205}$, and space group $P2_12_12_1$ with $a = 63.06$ Å, $b = 65.30$ Å, and $c = 101.39$ Å for $MKLN_{12–205}$.

Structure Solution

The structure of $MKLN_{1–205}$ was solved by sulfur SAD with the HySS (Hybrid Substructure Search) submodule of the Phenix package (Adams et al., 2002) together with the Oasis program of the CCP4 suite (Liu et al., 1999; Winn et al., 2011). The substructure was refined using SHARP (Bricogne et al., 2003), and iterations between automatically building partial models with the Buccaneer software (Cowtan, 2006) using the modified map and refinement of the partial model and density modification in SHARP finally led to an improved model, which was then completed manually and further refined using REFMAC (Skubak et al., 2004). Despite extensive rebuilding efforts, the structure could not be refined to an R_{free} below 34%. The structure of $MKLN_{12–205}$ was solved by molecular replacement with Phaser (McCoy et al., 2007) and refined with Phenix (Adams et al., 2002).

Biochemical Analyses

All biochemical analyses were performed in similar buffer conditions (20 mM PIPES, 200 mM NaCl, 5% glycerol [pH 7.5] supplied with either 5 mM dithiothreitol or 1 mM TCEP as reducing agent); more detailed descriptions are provided in the Supplemental Experimental Procedures. For SEC-MALS analysis the purified proteins were separated by SEC coupled in-line to MALS (DAWN 8+ HELEOS II, Wyatt Technology) and refractive index detectors (OptilabT-rEX, Wyatt Technology). Data were analyzed using the ASTRA software package (Wyatt Technology). For chemical crosslinking, samples were diluted to a concentration of 20 μM and pre-equilibrated before addition of the crosslinking reagent BS^3. The reaction was stopped by addition of Tris and all samples were analyzed by SDS-PAGE. For isothermal titration measurements, the variants of the discoidin domain ($MKLN_{1–156}$) were titrated into the cell containing $MKLN_{205–735}$ or buffer for control measurements, respectively, using a Microcal ITC200 instrument (GE Healthcare). Data were analyzed assuming a one-site binding model.

Surface Biotinylation Assay

The effect of muskelin and its variants on the surface level of $GABA_A$ receptor was assessed with a surface biotinylation assay performed as previously described (Heisler et al., 2011); details are provided in the Supplemental Experimental Procedures.

Intracellular Distribution Analysis

To analyze the intracellular distribution in HEK293 cells and hippocampal neurons, the cells were cotransfected with GFP and muskelin variants fused to either mRFP or mCherry. One day after transfection the cells were fixed, permeabilized, and treated with nucleic acid stain. Cells were imaged with a confocal fluorescent laser scanning microscope and classified according to the intracellular distribution of the red fluorescent signal into nuclear, mixed, or cytoplasmic localization. Statistical significance was assessed with Student's t test. Details on cell treatment, imaging, and image analysis are described in the Supplemental Experimental Procedures.

ACCESSION NUMBERS

The atomic coordinates and measured structure factor amplitudes for $MKLN_{12–205}$ have been deposited in the Protein Data Bank with accession code 4OYU.

SUPPLEMENTAL INFORMATION

Supplemental Information includes six figures, one table, and Supplemental Experimental Procedures and can be found with this article online at http://dx.doi.org/10.1016/j.str.2014.11.016.

ACKNOWLEDGMENTS

This work was supported by the Deutsche Forschungsgemeinschaft (FZ 82, SFB487 C7, and Schi 425/8-1 to H.S.; DFG KN556/6-1 and GRK1459 to M.K.). C.D. was supported by a grant of the German Excellence Initiative to the Graduate School of Life Sciences, University of Würzburg. We thank Petra Breiden and Yvonne Pechmann for technical assistance and Drs. Caroline Kisker and Daniela Schneeberger for critical reading of the manuscript. We acknowledge the Helmholtz Zentrum Berlin and the European Synchrotron Radiation Facility for provision of synchrotron radiation facilities and we would like to thank the staff of the BESSY at beamline 14.1 and the European Synchrotron Radiation Facility at beamline BM14 for technical assistance.

Received: April 24, 2014
Revised: November 6, 2014
Accepted: November 18, 2014
Published: January 8, 2015

REFERENCES

Adams, J.C., Seed, B., and Lawler, J. (1998). Muskelin, a novel intracellular mediator of cell adhesive and cytoskeletal responses to thrombospondin-1. EMBO J. *17*, 4964–4974.

Adams, P.D., Grosse-Kunstleve, R.W., Hung, L.W., Ioerger, T.R., McCoy, A.J., Moriarty, N.W., Read, R.J., Sacchettini, J.C., Sauter, N.K., and Terwilliger, T.C. (2002). PHENIX: building new software for automated crystallographic structure determination. Acta Crystallogr. D Biol. Crystallogr. *58*, 1948–1954.

Barral, D.C., and Seabra, M.C. (2004). The melanosome as a model to study organelle motility in mammals. Pigment Cell Res. *17*, 111–118.

Bricogne, G., Vonrhein, C., Flensburg, C., Schiltz, M., and Paciorek, W. (2003). Generation, representation and flow of phase information in structure determination: recent developments in and around SHARP 2.0. Acta Crystallogr. D Biol. Crystallogr. *59*, 2023–2030.

Cowtan, K. (2006). The Buccaneer software for automated model building. 1. Tracing protein chains. Acta Crystallogr. D Biol. Crystallogr. *62*, 1002–1011.

Davis, I.W., Murray, L.W., Richardson, J.S., and Richardson, D.C. (2004). MOLPROBITY: structure validation and all-atom contact analysis for nucleic acids and their complexes. Nucleic Acids Res. *32*, W615–W619.

Debenedittis, P., Harmelink, C., Chen, Y., Wang, Q., and Jiao, K. (2011). Characterization of the novel interaction between muskelin and TBX20, a critical cardiogenic transcription factor. Biochem. Biophys. Res. Commun. *409*, 338–343.

Emes, R.D., and Ponting, C.P. (2001). A new sequence motif linking lissencephaly, Treacher Collins and oral-facial-digital type 1 syndromes, microtubule dynamics and cell migration. Hum. Mol. Genet. *10*, 2813–2820.

Francis, O., Han, F., and Adams, J.C. (2013). Molecular phylogeny of a RING E3 ubiquitin ligase, conserved in eukaryotic cells and dominated by homologous components, the muskelin/RanBPM/CTLH complex. PLoS One *8*, e75217.

Gerlitz, G., Darhin, E., Giorgio, G., Franco, B., and Reiner, O. (2005). Novel functional features of the Lis-H domain: role in protein dimerization, half-life and cellular localization. Cell Cycle *4*, 1632–1640.

Hasegawa, H., Katoh, H., Fujita, H., Mori, K., and Negishi, M. (2000). Receptor isoform-specific interaction of prostaglandin EP3 receptor with muskelin. Biochem. Biophys. Res. Commun. *276*, 350–354.

Heisler, F.F., Loebrich, S., Pechmann, Y., Maier, N., Zivkovic, A.R., Tokito, M., Hausrat, T.J., Schweizer, M., Bähring, R., Holzbaur, E.L.F., et al. (2011). Muskelin regulates actin filament- and microtubule-based $GABA_A$ receptor transport in neurons. Neuron *70*, 66–81.

Kabsch, W. (2010). Xds. Acta Crystallogr. D Biol. Crystallogr. *66*, 125–132.

Kelley, L.A., and Sternberg, M.J.E. (2009). Protein structure prediction on the Web: a case study using the Phyre server. Nat. Protoc. *4*, 363–371.

Kiedzierska, A., Smietana, K., Czepczynska, H., and Otlewski, J. (2007). Structural similarities and functional diversity of eukaryotic discoidin-like domains. Biochim. Biophys. Acta *1774*, 1069–1078.

Kiedzierska, A., Czepczynska, H., Smietana, K., and Otlewski, J. (2008). Expression, purification and crystallization of cysteine-rich human protein muskelin in *Escherichia coli*. Protein Expr. Purif. *60*, 82–88.

Kim, M.H., Cooper, D.R., Oleksy, A., Devedjiev, Y., Derewenda, U., Reiner, O., Otlewski, J., and Derewenda, Z.S. (2004). The structure of the N-terminal domain of the product of the lissencephaly gene Lis1 and its functional implications. Structure *12*, 987–998.

Kobayashi, N., Yang, J., Ueda, A., Suzuki, T., Tomaru, K., Takeno, M., Okuda, K., and Ishigatsubo, Y. (2007). RanBPM, Muskelin, p48EMLP, p44CTLH, and the armadillo-repeat proteins ARMC8α and ARMC8β are components of the CTLH complex. Gene *396*, 236–247.

Krissinel, E., and Henrick, K. (2007). Inference of macromolecular assemblies from crystalline state. J. Mol. Biol. *372*, 774–797.

Ledee, D.R. (2005). A specific interaction between muskelin and the cyclin-dependent kinase 5 activator p39 promotes peripheral localization of muskelin. J. Biol. Chem. *280*, 21376–21383.

Leslie, A.G.W., and Powell, H.R. (2007). Processing diffraction data with Mosflm. In Evolving Methods for Macromolecular Crystallography, R.J. Read and J.L. Sussman, eds. (Dordrecht: Springer), pp. 41–51.

Liu, Y.D., Gu, Y.X., Zheng, C.D., Hao, Q., and Fan, H.F. (1999). Combining direct methods with isomorphous replacement or anomalous scattering data. VIII. Phasing experimental SIR data with the replacing atoms in a centrosymmetric arrangement. Acta Crystallogr. D Biol. Crystallogr. *55*, 846–848.

Mateja, A., Cierpicki, T., Paduch, M., Derewenda, Z.S., and Otlewski, J. (2006). The dimerization mechanism of LIS1 and its implication for proteins containing the LisH motif. J. Mol. Biol. *357*, 621–631.

McCoy, A.J., Grosse-Kunstleve, R.W., Adams, P.D., Winn, M.D., Storoni, L.C., and Read, R.J. (2007). Phaser crystallographic software. J. Appl. Crystallogr. *40*, 658–674.

Mikolajka, A., Yan, X., Popowicz, G.M., Smialowski, P., Nigg, E.A., and Holak, T.A. (2006). Structure of the N-terminal domain of the FOP (FGFR1OP) protein and implications for its dimerization and centrosomal localization. J. Mol. Biol. *359*, 863–875.

Oberoi, J., Fairall, L., Watson, P.J., Yang, J.C., Czimmerer, Z., Kampmann, T., Goult, B.T., Greenwood, J.A., Gooch, J.T., Kallenberger, B.C., et al. (2011). Structural basis for the assembly of the SMRT/NCoR core transcriptional repression machinery. Nat. Struct. Mol. Biol. *18*, 177–184.

Prag, S., Collett, G.D.M., and Adams, J.C. (2004). Molecular analysis of muskelin identifies a conserved discoidin-like domain that contributes to protein self-association. Biochem. J. *381*, 547–559.

Prag, S., De Arcangelis, A., Georges-Labouesse, E., and Adams, J. (2007). Regulation of post-translational modifications of muskelin by protein kinase C. Int. J. Biochem. Cell Biol. *39*, 366–378.

Qin, S., and Zhou, H.X. (2007). meta-PPISP: a meta web server for protein-protein interaction site prediction. Bioinformatics *23*, 3386–3387.

Regelmann, J., Schule, T., Josupeit, F.S., Horak, J., Rose, M., Entian, K.D., Thumm, M., and Wolf, D.H. (2003). Catabolite degradation of fructose-1,6-bisphosphatase in the yeast *Saccharomyces cerevisiae*: a genome-wide screen identifies eight novel GID genes and indicates the existence of two degradation pathways. Mol. Biol. Cell *14*, 1652–1663.

Rodionov, V., Yi, J., Kashina, A., Oladipo, A., and Gross, S.P. (2003). Switching between microtubule- and actin-based transport systems in melanophores is controlled by cAMP levels. Curr. Biol. *13*, 1837–1847.

Skubak, P., Murshudov, G.N., and Pannu, N.S. (2004). Direct incorporation of experimental phase information in model refinement. Acta Crystallogr. D Biol. Crystallogr. *60*, 2196–2201.

Tagnaouti, N., Loebrich, S., Heisler, F., Pechmann, Y., Fehr, S., De Arcangelis, A., Georges-Labouesse, E., Adams, J.C., and Kneussel, M. (2007). Neuronal expression of muskelin in the rodent central nervous system. BMC Neurosci. *8*, 28.

Umeda, M., Nishitani, H., and Nishimoto, T. (2003). A novel nuclear protein, Twa1, and Muskelin comprise a complex with RanBPM. Gene *303*, 47–54.

Valiyaveettil, M., Bentley, A.A., Gursahaney, P., Hussien, R., Chakravarti, R., Kureishy, N., Prag, S., and Adams, J.C. (2008). Novel role of the muskelin-RanBP9 complex as a nucleocytoplasmic mediator of cell morphology regulation. J. Cell Biol. *182*, 727–739.

Vithlani, M., Terunuma, M., and Moss, S.J. (2011). The dynamic modulation of $GABA_A$ receptor trafficking and its role in regulating the plasticity of inhibitory synapses. Physiol. Rev. *91*, 1009–1022.

Watabe, H., Valencia, J.C., Le Pape, E., Yamaguchi, Y., Nakamura, M., Rouzaud, F., Hoashi, T., Kawa, Y., Mizoguchi, M., and Hearing, V.J. (2008). Involvement of dynein and spectrin with early melanosome transport and melanosomal protein trafficking. J. Invest. Dermatol. *128*, 162–174.

Wen, J., Arakawa, T., and Philo, J.S. (1996). Size-exclusion chromatography with on-line light-scattering, absorbance, and refractive index detectors for studying proteins and their interactions. Anal. Biochem. *240*, 155–166.

Winn, M.D., Ballard, C.C., Cowtan, K.D., Dodson, E.J., Emsley, P., Evans, P.R., Keegan, R.M., Krissinel, E.B., Leslie, A.G., McCoy, A., et al. (2011). Overview of the CCP4 suite and current developments. Acta Crystallogr. D Biol. Crystallogr. *67*, 235–242.

Wu, W.W., Wong, J.P., Kast, J., and Molday, R.S. (2005). RS1, a discoidin domain-containing retinal cell adhesion protein associated with X-linked retinoschisis, exists as a novel disulfide-linked octamer. J. Biol. Chem. *280*, 10721–10730.